Chapter 6
THERMAL STABILITY AND SELF-ARRANGEMENT OF NANOCRYSTALLINE HARD COATINGS

P. H. Mayrhofer
Department of Physical Metallurgy and Materials Testing, University of Leoben, 8700 Leoben, Austria

Nanocrystalline hard coatings have attracted increasing interest in modern development of hard coatings. Their increased volume fraction of interfaces is often responsible for superior properties, but they stimulate also microstructural processes. Whereas for single-phase coatings a remarkable reduction in hardness occurs around 500°C, nanocomposites maybe stable up to 1000°C. In physical vapor deposited (PVD) hard coatings nanostructures can arise during growth or during a post annealing treatment. In non-reactively sputtered overstoichiometric TiB_2 coatings the excess of boron forms a tissue phase surrounding TiB_2 crystals. Thus, a nanocolumnar structure with a diameter of about 5 nm is formed during the deposition process. Another example for segregation driven formation of a nanostructure is TiN-TiB_2, where the coating consists mainly of TiN and TiB_2 nanocrystals of about 3 nm due to their extremely limited solubility. Nanostructures can also arise during annealing of supersaturated coatings. Thermal treatment of $Ti_{1-x}Al_xN$ coatings causes the metastable phase to decompose into its stable constituents TiN and AlN. Initially $Ti_{1-x}Al_xN$ coatings undergo spinodal decomposition generating an increase in hardness at elevated temperatures. The results presented show that next generation's coatings with increased ability for self-arrangement can effectively be prepared by PVD.

Keywords: hardening, nanocomposite, spinodal decomposition, thermal stability, self-arrangement.

1. INTRODUCTION

In the last few years, several hard coating materials with unique properties have been developed or even transferred to industrial applications. Essentially, two different coating material groups can be distinguished. The first one includes materials with inherent unique properties, e.g., diamond-like carbon DLC [1], diamond [2] and cubic boron nitride [3] as inherently hard or even superhard (where the hardness exceeds 40 GPa) materials or aluminum oxide as thermally extremely stable coating [4]. The second group covers heterostructures. Unlike the multilayer coatings like the commercially

A. A. Voevodin et al. (eds.),
Nanostructured Thin Films and Nanodispersion Strengthened Coatings, 57–68.

applied TiC-Al_2O_3-TiN coatings deposited by CVD techniques with layer thicknesses in the order of a few to several tenth of microns [5], nanoscaled heterostructures allow the design of unique properties or property combinations. The first attempts to deposit these structures have been made with the goals (1) to create new superhard materials (see e.g., the review by Vepřek [6]) or to combine properties like high hardness with (2) high toughness [7] or (3) a low friction coefficient [8,9]. The latter task focuses on the design of functional coatings where nanodispersive structures consisting of hard (e.g., TiN) and lubricant phases (e.g., DLC, MoS_2) have been suggested. Here, this topic will not be discussed further. This paper mainly deals with the optimization of mechanical properties represented by hardness and its thermal stability by the formation of heterostructures, which arrange themselves during growth of the coating or during a thermal treatment after deposition.

The science of materials is to a large extend couched in terms of length scales and their interactions. Thus, the mechanical response of materials can be understood from the point of view of the interaction of a characteristic length, which may be the dislocation radius at a given stress, with a size parameter describing the microstructure (e.g., grain size, column diameter, particle size, film thickness) [10]. Hardening of metals is caused by providing obstacles for the dislocation movement, these mechanisms can also be applied to some extent to hard coatings. Hindering of dislocation movement can be achieved by, (1) high density of point and line defects generated by energetic ion bombardment during growth, (2) internal boundaries like grain and column boundaries, (3) second phase particles and (4) solutes. Solutes in a crystal act as obstacles to dislocation motion through their elastic and/or chemical interactions with dislocations. Most solutes are weak hardeners except for the (technologically) important class of interstitial solutes that induce anisotropic distortions of the lattice. Second phase particles are generally the most potent strengthening agent in practical high strength engineering materials, their mechanisms can be divided into coherency, chemical, order, stacking-fault and modulus hardening [11,12].

The different mechanisms are individual in their effectiveness of hardening and especially in their effectiveness during a thermal treatment, which will be discussed in the following chapters.

2. THERMAL STABILITY OF SINGLE-PHASE HARD COATINGS

In single phase hard coatings like TiN a hardness increase can be obtained either by high energetic bombardment during growth of the films causing high compressive stresses or by a reduction of the grain size [13]. The effect of smaller grain sizes on the yield stress is classically described

by the Hall-Petch relationship which is based on dislocation pile-up at grain boundaries. The dependence of hardness of single-phase TiN coatings on their compressive biaxial stresses generated by ion bombardment during growth can be seen in Fig. 1a. Using this method even hardness values of about 56 GPa for TiN can be achieved, but their compressive stresses are extremely high [14]. These high stresses are an additional driving force for recovery effects [15] during a thermal treatment of the coatings. Thus, the onset-temperature where annihilation of defects in the coatings occur decreases (cf. Fig. 1b). As soon as the onset-temperature of recovery is reached the hardness of single-phase TiN coatings decreases as point and line defects anneal which determine the hardness of such coatings to a high extent [14,16].

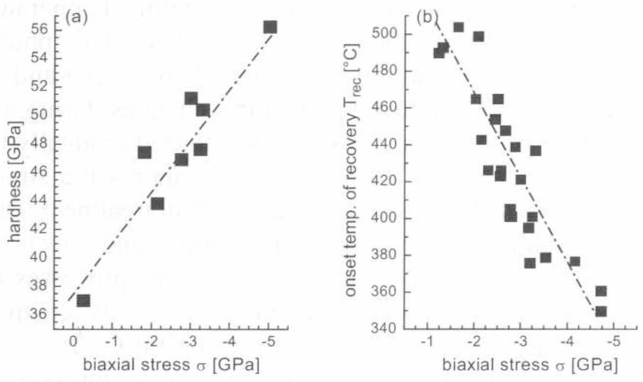

Figure 1. (a) Hardness and (b) onset temperature of recovery as a function of the biaxial compressive stresses in non-reactively sputtered TiN coatings.

Thus, the hardening mechanism for coatings by high-energetic bombardment during growth is not suitable to obtain high hot hardness due to decreasing onset-temperature for recovery [14,17]. Other hardening mechanism like internal boundaries, second phase particles and solutes as mentioned above seem to be much more promising to obtain high hardness which sustains also higher temperatures [17-19]. These mechanisms can be effective due to self-arranging nanostructures either during coating growth an annealing treatment afterwards e.g., during coating operation. The following sections provide some examples to this topic.

3. SELF-ARRANGING NANOSTRUCTURES DURING GROWTH

In 1995, Vepřek and co-workers [18] presented their model on the design of novel superhard nanocomposite coating materials. Using PACVD, they

deposited coatings within the system TiN-Si_3N_4 where nanocrystals of TiN due to a segregation driven renucleation are embedded in an amorphous matrix. For these coatings they achieved superhardness values of 80 to 105 GPa [19]. They showed also clearly, that hardness values which are mainly the result of nanostructure sustain higher temperatures than those which are obtained by high energetic bombardment during growth as mentioned above. A very interesting hard coating is TiB_2 [20], which is assumed to be single phase but this coating shows also high hardness even after annealing in vacuum at 800°C. By non-reactive sputtering from a sintered TiB_2 target it was found, that the chemical composition strongly depends on the ion bombardment during growth. Thus, B/Ti ratios between 2.45 and 3.15 could be achieved simply by increasing the ion/atom flux ratio from 1 to 20 at constant ion energy of 30 eV [21]. Figure 2a shows the XRD evolution of such a superstoichiometric TiB_2 coating with annealing temperature. The patterns indicate a well defined (0001) orientation of the TiB_2 phase which remains unchanged for all annealing temperatures. Broadening and intensity of the <0001> peaks indicate almost no structural changes during a thermal treatment up to 800°C, although the peak position shifted gradually to higher diffraction angles. This indicates a reduction of compressive stresses and even the appearance of tensile stresses after the thermal treatment. Due to the different thermal expansion coefficient of coating and steel substrate combined with the stress reduction caused by recovery processes and out-annealing of argon, the highly covalent and thus brittle TiB_2 coating shows crack formation if the annealing temperature exceeds 700°C [21].

Although, there is unambiguously a reduction of compressive stresses during annealing, their hardness remains essentially constant (see Fig. 2b). The results obtained are completely different to single-phase nitride films, where a distinct reduction of their hardness with annealing temperature appears as mentioned above. For comparison data of TiN are added to Fig. 2b. Accompanied with this hardness decrease there is always a pronounced structural change (e.g., defect density, orientation, and grain size) of the coatings caused by recovery and recrystallization processes [14,16]. The investigated overstoichiometric TiB_2 coatings do not show these structural changes during an annealing treatment up to 800°C, excluding the decreasing compressive stresses. This behavior emphasizes, that their hardness is mainly determined by their micro- or nano-structure, and not by compressive stresses. Recent investigations showed, that the excess of boron resulting from non-reactive sputtering forms a tissue phase due to the extremely limited composition range of the TiB_2 phase. In the TiB_2 lattice, a surplus of boron would generate extremely high strain fields. Therefore, the TiB_2 lattice accommodates itself by segregating boron which forms a tissue phase embedded in almost stoichiometric TiB_2. This tissue phase draws through the whole coating and is elongated in the growth direction, thus causes the formation of nanocolumns with an average diameter of 5 nm [21].

The results show that non-reactively sputtered overstoichiometric TiB_2 coatings do not pertain to single-phase coatings. In this way the origin of the extraordinary high hardness of this class of material and their thermal stability can be explained. These findings are in good agreement to previous results about nanocomposite coatings showing that high hardness is obtained when the crystallite size is about 5 nm and a fully percolated amorphous phase separates the crystallites by approximately 0.5 nm [6,22,23].

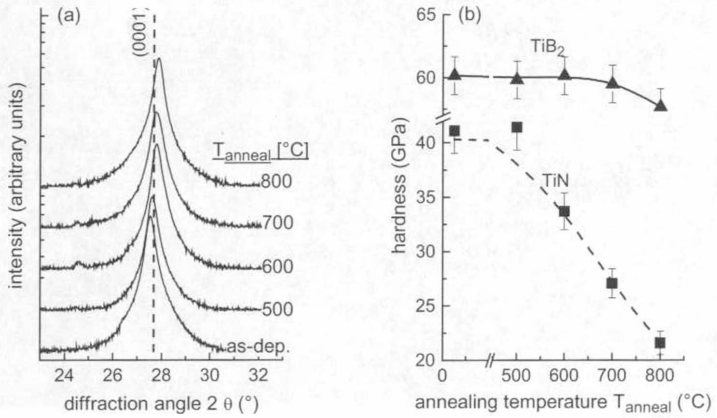

Figure 2. Thermal stability of the TiB_2 coating. (a) XRD patterns in the as-deposited state (as-dep.) and after different annealing temperatures (T_{anneal}). (b) Hardness evolution of TiB_2 as a function of annealing temperature compared to TiN.

Another method to form nanocomposite [24] coatings is co-sputtering of two immiscible phases like TiN and TiB_2 [25,26]. An example of such a coating, which was non-reactively co-sputtered from a segmented TiN-TiB_2 target is given in Fig. 3 which shows the nanostructure of the coating in the as-deposited state with a chemical composition of Ti = 36.5 at-%, B = 36 at-% and N = 27.5 at-% detected by EPMA measurements. In the bright field HRTEM micrograph (Fig. 3a) grains with an average size of about 3 nm can clearly be seen. The diffraction rings in the SAED pattern of the coating shown in Fig. 3b attribute to a possible mixture of TiN and TiB_2 nanocrystals [27]. But due to the limited local resolution or the formation of supersaturated Ti-B-N phases, lattice deformation and amorphous material no clear relation to the individual phases can be found. The z-contrast image (Fig. 3c) shows clearly a random orientation through the whole coating of at least two different phases. The bright dots indicate the appearance of a phase with a higher density than compared to the phase represented by the darker dots. Again the grain size can be estimated to be about 3 nm. Considering the extremely short diffusion paths in 3 nm grains to the nearest sink (i.e., grain and phase boundary) for defects almost 'perfect' crystals should form

during the deposition [27]. Thus, the coating is assumed to consist mainly of TiB_2 and TiN crystals with minor defects like incorporated N and B, respectively. In such nanocomposites with an average grain size of about 3 nm also the 'amorphous' phase surrounding the crystals plays an important role in determining the coatings properties.

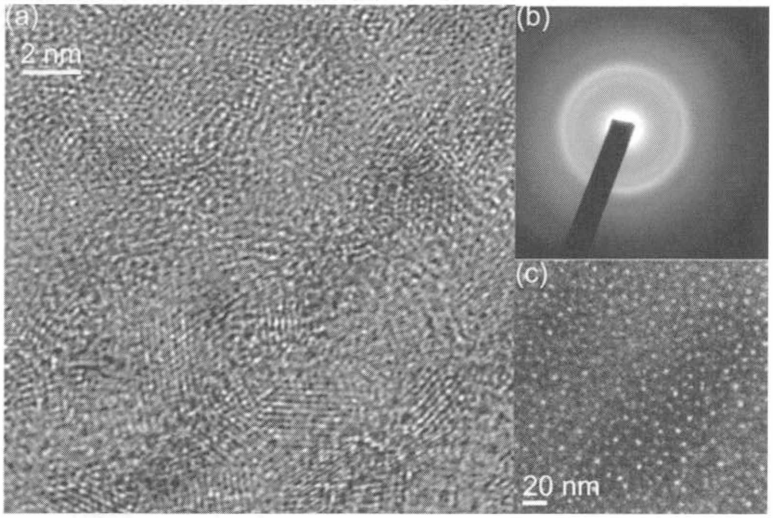

Figure 3. (a) Cross-sectional HRTEM bright field image of $TiB_1N_{0.75}$. (b) SAED pattern with diffraction rings corresponding to a mixture of amourphous phase and TiN and TiB_2 nanocrystals. (c) Z-contrast image indicating a random arrangement of two different phases.

Figure 4 shows a schematic drawing of the nucleation and growth process of the nanocomposite TiN-TiB_2 coating, indicating a self-arranging nanostructure due to segregation driven inhibited growth of the individual nuclei and renucleation, according to oxygen in Al coatings [28,29].

Since there is a high amount of amorphous material in the $TiB_1N_{0.75}$ coating, thermal treatment causes a rearrangement of the nanostructure due to on-crystallization of atoms from this amorphous phase to neighboring TiN and TiB_2 crystals. Thus, the structure and consequently the properties change by thermal treatment, which can occure during operation.

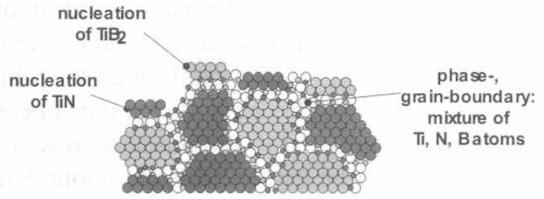

Figure 4. Schematic representation of the nucleation and growth process of $TiB_1N_{0.75}$, indicating segregation driven renucleation of TiN and TiB_2.

4. SELF-ORGANIZED NANOSTRUCTURES DURING THERMAL TREATMENT (OPERATION)

The thermal stability of the TiN-TiB_2 coating is shown in Fig. 5 represented by the XRD and hardness evolution with temperature. In the as-deposited state the broad XRD peaks can be the result of overlapped broad TiN and TiB_2 peaks, indicating a small grain size and a huge amount of amorphous material. After annealing at different temperatures the two phases TiN and TiB_2 become more pronounced indicated by more developed XRD peaks. Especially after an annealing treatment at 900°C a clear separation of the broad XRD peak into TiN and TiB_2 can be seen. After annealing treatment at 1400°C in argon atmosphere, where the coating was removed from the substrate to avoid interdiffusion a fully recrystallized structure containing just TiN and TiB_2 phases can be seen. Corresponding to nanostructural changes within the coating during annealing also the hardness

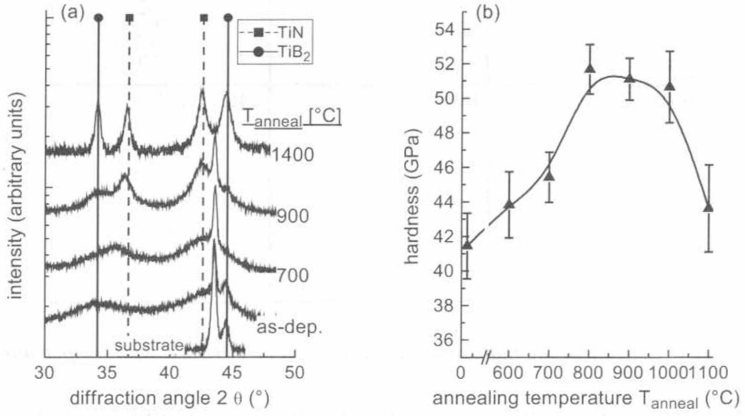

Figure 5. Thermal stability of $TiB_1N_{0.75}$. (a) XRD patterns after different annealing temperatures (T_{anneal}). (b) Hardness evolution with temperature.

changes with temperature (Fig. 5b). An increase from about 41 to about 51 GPa can be obtained by an annealing treatment up to 800 °C. If the annealing temperature exceeds 1000°C the coating hardness decreases due to recrystallization effects [15,27].

Figure 6 shows the nanostructural evolution of the coating for annealing temperatures of 700, 900, 1000, 1100 and 1400°C obtained from HRTEM investigations [27]. After a heat treatment at 700°C slight increase of the average grain size and a reduction of the amorphous phase surrounding the crystals can be observed in comparison to the as-deposited structure. Further increasing grain size and reduction of the amorphous phase is obtained if the

temperature is increased to 900 or 1000°C. After annealing at 1000°C the crystals are about 5...7 nm and separated by a thin boundary structure with just a few atoms in thickness. Atoms from the amorphous region crystallize onto the surrounded TiN and TiB_2 crystals. By a reduction of the amorphous phase the cohesive energy between the phases increases and grain boundary sliding is more difficult resulting in an increased hardness of the composite (cf. Fig. 5b). Again the highest hardness is obtained when the crystallite size is about 5 nm and a fully percolated amorphous phase separates the crystallites by approximately 0.5 nm [6,22,23]. At temperatures higher than 1000°C recrystallization and subsequent grain growth occurs resulting in grain sizes above 7 nm [30]. These processes are responsible for the observed hardness decrease if the heat treatment exceeds temperatures of 1000°C.

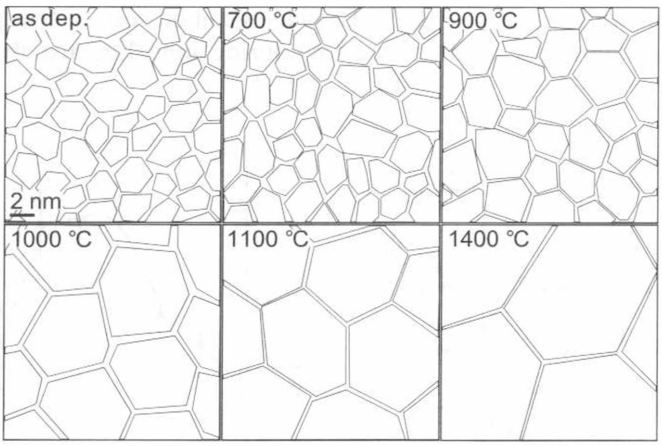

Figure 6. Scheme of the nanostructural evolution of $TiB_1N_{0.75}$ with temperature.

Additional confirmation, that the coating is mainly composed of nanocrystals of the stable phases TiN and TiB_2 surrounded by an amorphous region (mixture of Ti, B and N atoms) is given by DSC measurements since just two main exothermic peaks appear during a thermal treatment in argon atmosphere up to 1450°C (see Fig. 7a). These peaks could be identified to be the result of recovery and grain growth including crystallization effects of the amorphous region onto the surrounded nanocrystals [30]. The latter is represented by a huge asymmetric peak, elucidated in Fig. 7a, following the JMA theory [31]. The two narrow exothermic peaks between 600 and 1000°C could indicate, that the coating has also small amounts of additional supersaturated metastable phases like Ti-B-N which decompose into their stable constituents similar to $Ti_{1-x}Al_xN$ coatings [32]. In the as-deposited state, these coatings show a supersaturated $Ti_{1-x}Al_xN$ solid solution with NaCl-structure [34]. This metastable phase tends to decompose into the

stable phases face centered cubic (fcc) TiN and hexagonal close packed (hcp) AlN due to their extremely limited solubility [32-35].

Such structural changes are closely related to changes in total free-energy, that can be detected by DSC. During heating of the $Ti_{1-x}Al_xN$ coatings, four exothermic reactions (recovery, spinodal decomposition [36] to form fcc-AlN and TiN domains and subsequent recrystallization including the transformation of AlN from fcc to hcp) indicated in Fig. 7b were observed, whereas for TiN just one tiny peak appeared. XRD and TEM investigations prior to and after this exothermic peak of TiN indicated recovery processes of deposition-induced lattice point defects that correspond to a compressive residual stress state. Such structural relaxations explain the observed hardness decrease at temperatures higher than 400°C (cf. Fig. 2b) [14,33].

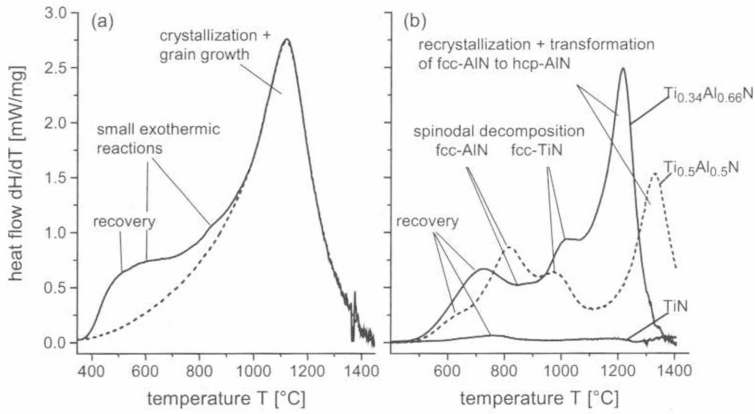

Figure 7. Dynamical DSC measurements of hard coatings. (a) DSC curve of non-reactively sputtered $TiB_1N_{0.75}$. (b) DSC curve of arc-evaporated $Ti_{0.5}Al_{0.5}N$ and $Ti_{0.34}Al_{0.66}N$ coatings compared to arc-evaporated TiN.

After recovery the supersaturated $Ti_{1-x}Al_xN$ coatings initially undergo spinodal decomposition into coherent fcc-AlN and fcc-TiN nanometer-size domains. This transformation generates an increase in hardness at elevated temperatures (age hardening [11,12]), e.g., during cutting. Therefore, the hardness of $Ti_{0.34}Al_{0.66}N$ coatings show a slight hardness increase between 700 and 950°C. The structure can thus be said to self-organize during thermal loading such as in cutting operations. Further decomposition causes a coarsening of the domains and eventual precipitation into the equilibrium fcc-TiN and hcp-AlN phases, and a resulting hardness decrease at temperatures over 950°C for $Ti_{0.34}Al_{0.66}N$ (overaging [11,12]). From detailed investigations of the structural transformations during a thermal treatment it is known, that the coatings start with the formation of Al rich domains ($TiAl_{1+\Delta}N$) thus, in their vicinity the coating shows Al deficiency ($TiAl_{1-\Delta}N$) indicated in Fig. 8. Such segregation amounts to uphill diffusion, i.e.

diffusion in the opposite direction of the concentration gradient (i.e., spinodal decomposition). A schematic representation of the decomposition process of supersaturated $Ti_{1-x}Al_xN$ coatings and the appearance of coherency strains is given in Fig. 8. Differences in the lattice parameter

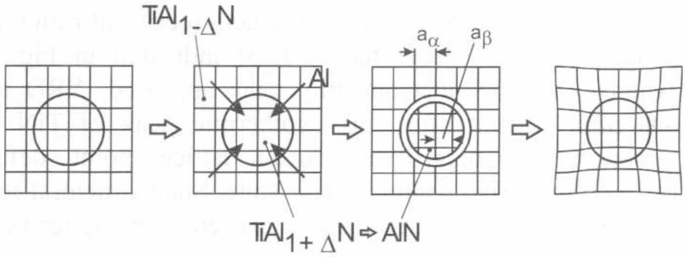

Figure 8. Schematic drawing of the spinodal decomposition process of a supersaturated TiAlN coating and the origin o coherency stresses.

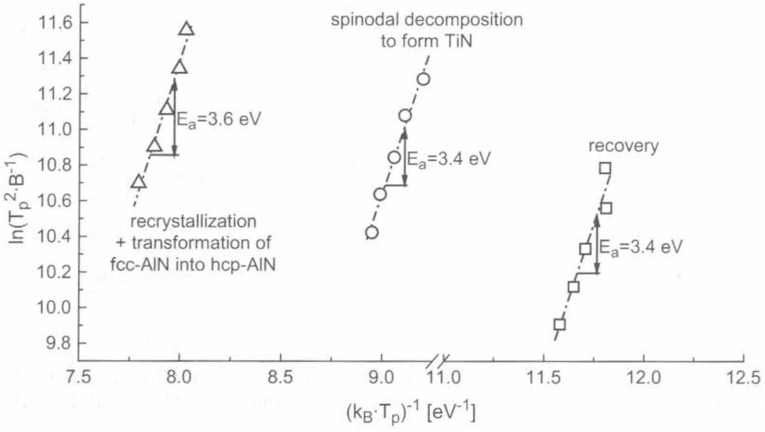

Figure 9. Kissinger analysis of the effective activation energy for recovery, decomposition and recrystallization of a $Ti_{0.34}Al_{0.66}N$ coating, calculated from the change in peak temperature (T_p) with heating rate (B) of the DSC measurement.

between newly formed domain (a_β) and remaining matrix (a_α), give rise to elastic stresses in the vicinity of the domain due to coherency stresses which act as obstacles for dislocations causing a hardening of the material during thermal treatment (i.e., age hardening).

5. CONCLUSION

Activation energies for the exothermic reactions shown in Fig. 7b (i.e., recovery, spinodal decomposition, and recrystallization) in a $Ti_{0.34}Al_{0.66}N$ coating were determined by Kissinger plots (see Fig. 9) using the respective peak temperature for different heating rates during DSC.

The activation energies for recovery and the formation of TiN domains are very similar and yield values of 3.4 eV. Recovery and spinodal decomposition are diffusion-controlled within one phase without nucleation, thus explaining the similar values. For the fcc-hcp transformation of AlN and subsequent recrystallization of the coatings, additional nucleation is needed resulting in a slightly higher activation energy of 3.6 eV [32]. Interestingly, the activation energy for surface diffusion of Ti on TiN was determined to be 3.5 eV [38]. The similar values obtained for diffusional phase transformation in the bulk imply a defect-driven process from, e.g., dislocations, which are present at high densities in the coatings.

Several mechanims of hardening for PVD coatings were investigated in detail. It could be shown, that hardening of coatings by a high density of point and line defects generated by an intense ion bombardment during deposition is not suitable to obtain a high hot hardness. These defects may easily anneal during thermal treatment, e.g. in coating operation.

Hindering of dislocation movement by internal boundaries and second phase particles is much more effective to obtain high hardness which sustains higher temperatures or even increases with temperature. These mechanisms can be effective due to nanosructure self-arranging in growth and/or in thermal treatment (e.g. during coating operation). Examples for self-arranging nanostructures during growth are supersaturated TiB_2, where the surplus of boron causes formation of nanocolumns, and co-sputtered TiN-TiB_2, where a segregation driven nanostructure forms by renucleation. During a thermal treatment of the latter one their nanostructure arranges itself due to the on-crystallization of additional amorphous phase present in the as-deposited state causing an hardness increase with temperature.

Age hardening in hard coatings, as shown for supersaturated $Ti_{1-x}Al_xN$, is very effective to obtain high hardness at increased temperatures. During annealing, this class of materials decomposes into stable constituents, where coherent cubic AlN-rich and TiN-rich domains are formed by spinodal decomposition during early stages of phase-separation. Further aging results in coarsening of these domains to form separated fcc-TiN and fcc- and finally hcp-AlN phases. If dislocations are able to bow between these obstacles, a hardness decrease is observed.

The results presented show, that by choosing the proper elements for hard coatings high hot hardness can be designed using different mechanisms and knowing the underlying materials science.

ACKNOWLEDGMENTS

The Center for Microanalysis of Materials which is partially supported by the U.S. Department of Energy (DOE), at the University of Illinois is highly acknowledged.

REFERENCES

1. A. Grill, Diam. Relat. Mater. 8 (1999) 428.
2. C. Faure, W. Hänni, C. J. Schmutz, M. Gervanoni, Diam. Relat. Mater. 8 (1999) 830.
3. P. B. Mirkarimi, K. F. McCarty, D. L. Medlin, Mater. Sci. Engin. Reports 21 (1997) 47.
4. J. M. Schneider, W. D. Sproul, A. Matthews, Surf. Coat. Technol. 98 (1998) 1473.
5. W. Schintlmeister, W. Wallgram, J. Kanz, K. Gigl, Wear 100 (1984) 153.
6. S. Vepřek, J. Vac. Sci. Technol. A 17 (1999) 2401.
7. H. Holleck, V. Schier, Surf. Coat. Technol. 76-77 (1995) 328.
8. A. A. Voevodin, J. P. O'Neill, J. S. Zabinski, Surf. Coat. Technol. 116-119 (1999) 36.
9. R. Gilmore, M. A. Baker, P. N. Gibson, W. Gissler, M. Stoiber, P. Losbichler, C. Mitterer, Surf. Coat. Technol. 108-109 (1998) 345.
10. E. Arzt, Acta. Mater. 46 (1998) 5611.
11. P. Haasen, Physical Metallurgy, Univ. Press, Cambridge, 1986.
12. D. A. Porter, K. E. Easterling, Phase Transformations in Metals and Alloys, Stanley Thornes, Cornwall, 2000.
13. I. Petrov, L. Hultman, J.-E. Sundgren, J. E. Greene, J. Vac. Sci. Technol. A 10(2) (1992) 265.
14. P. H. Mayrhofer, F. Kunc, J. Musil, C. Mitterer, Thin Solid Films 415 (2002) 151.
15. F. J. Humphreys, M. Hatherly, Recrystallization and Related Annealing Phenomena, Elsevier, Oxford, 1995.
16. L. Hultman, Vacuum 57 (2000) 1.
17. H.-D. Männling, D. S. Patil, K. Moto, M. Jílek, S. Vepřek, Surf. Coat. Technol. 146-147 (2001) 263.
18. S. Vepřek, S. Reiprich., Thin Solid Films 268 (1995) 64.
19. A. Niederhofer, P. Nesládek, H.-D. Männling, K. Moto, S. Vepřek, M. Jílek, Surf. Coat. Technol. 120-121 (1999) 173.
20. C. Mitterer, J. Sol. State Chem. 133 (1997) 279.
21. P. H. Mayrhofer, J. G. Wen, I. Petrov, C. Mitterer, J. E. Greene, Appl. Phys. Lett. submitted.
22. S. Vepřek, A. S. Argon, J. Vac. Sci. Technol. B 20(2) (2002) 650.
23. J. Patscheider, T. Zehnder, M. Diserens, Surf. Coat. Technol. 146-147 (2001) 201.
24. J. Musil, Surf. Coat. Technol. 125 (2000) 322.
25. C. Mitterer, P. Losbichler, F. Hofer, P. Warbichler, P.N. Gibson, W. Gissler, Vacuum 50(3-4) (1998) 313.
26. P. Losbichler, C. Mitterer, P. N. Gibson, W. Gissler, F. Hofer, P. Warbichler, Surf. Coat. Technol. 94-95 (1997) 297.
27. P. H. Mayrhofer, C. Mitterer, J. G. Wen, I. Petrov, J. E. Greene, in preparation.
28. P. B. Barna, M. Adamik, Thin Solid Films 317 (1998) 27.
29. I. Petrov, P. B. Barna, L. Hultman, J. E. Greene, J. Vac. Sci. Technol. A 21(5) (2003) 117.
30. P. H. Mayrhofer, H. Willmann, C. Mitterer, Thin Solid Films 440 (2003) 174.
31. C. Michaelsen, K. Barmak, T. P. Weihs, J. Phys. D: Appl. Phys. 30 (1997) 3167.
32. P. H. Mayrhofer, A. Hörling, L. Karlsson, J. Sjölén, C. Mitterer, L. Hultman, Appl. Phys. Lett. 83 (2003) 2049.
33. A. Hörling, L. Hultman, M. Odén, J. Sjölen, L. Karlsson, J. Vac. Sci. Technol. A 20 (5) (2002) 1815.
34. W.-D. Münz, J. Vac. Sci. Technol. A 4 (6) (1986) 2717.
35. S. PalDey, S. C. Deevi, Mat. Sci. Engin. A 342 (1-2) (2002) 58.
36. J. W. Cahn, Acta Met. 9 (1961) 795.
37. H.E. Kissinger, Anal. Chem., 29 (1957) 1702.
38. S. Kodambaka, V. Petrova, A. Vailionis, P. Desjardins, D. G. Cahill, I. Petrov, J. E. Greene, Thin Solid Films 392 (2001) 164.